# Solar flare physics

## Boris V. Somov

Solar Physics Department, Astronomical Institute, Moscow State University, Universitetskii
Prospekt 13, Moscow 119992, Russia  email: somov@sai.msu.ru

**Abstract.** Specific features of magnetic reconnection in solar flares are briefly reviewed and
illustrated. In particular, the large-scale structure and dynamics of large flares are interpreted
in terms of the rainbow reconnection model. The role of the betatron effect in collapsing magnetic
traps is considered.

## 1. Introduction

The potential part of magnetic field in the solar corona determines a large-scale struc-
ture of flare-active regions, while the reconnecting current layers (RCLs) at separators,
together with other non-potential components of the field, determine energetics and dy-
namics of flares (e.g. Somov et al. 2003). The basic properties of magnetic reconnection
in solar flares are summarized in § 2. In § 3, the first-order Fermi-type acceleration and
betatron effect in the collapsing magnetic traps, that are created by reconnection in the
solar atmosphere, are considered.

## 2. Main features of reconnection in flares

### 2.1. *Collisionless magnetic reconnection*

Coulomb collisions do not play any role in RCLs of a flare because of very high (super-
hot) temperature of a plasma inside a RCL. Hence, this plasma must be considered as
essentially collisionless. The concept of collisionless reconnection describes well the fast
conversion from magnetic field energy to particle energy. That is what we need, first of
all, to explain high power of flares.

Powerful direct heating of electrons and ions results from wave-particle interactions
inside a super-hot turbulent-current layer (SHTCL). A particular feature of the SHTCL
model (Somov 2000) is that electrons and ions are heated in a different way:

$$\chi_{\mathrm{ef}}\, \mathcal{E}_{mag}^{in} + \mathcal{E}_{th,e}^{in} = \mathcal{E}_{th,e}^{out} + \mathcal{C}_{\parallel}^{an}\,, \tag{2.1}$$

$$(1 - \chi_{\mathrm{ef}})\, \mathcal{E}_{mag}^{in} + \mathcal{E}_{th,i}^{in} = \mathcal{E}_{th,i}^{out} + \mathcal{K}_{i}^{out}\,. \tag{2.2}$$

The left-hand sides of the energy equations for electrons (2.1) and ions (2.2) contain the
magnetic energy flux

$$\mathcal{E}_{mag}^{in} = \frac{B_0^2}{4\pi}\, v_0\, b\,, \tag{2.3}$$

which coincides with the direct heating of the ions and electrons due to their interactions
with waves; $b$ is a half-width of the layer (figure 1). A relative fraction $\chi_{\mathrm{ef}}$ of the heating
is consumed by electrons, while the remaining fraction $(1 - \chi_{\mathrm{ef}})$ goes to the ions.

The electron and ion temperatures of the plasma inflowing to the layer are the same.
Hence, the fluxes of the electron and ion thermal energies are also the same:

$$\mathcal{E}_{th,e}^{in} = \mathcal{E}_{th,i}^{in} = \frac{5}{2}\, n_0 k_{\mathrm{B}} T_0 \cdot v_0 b\,. \tag{2.4}$$
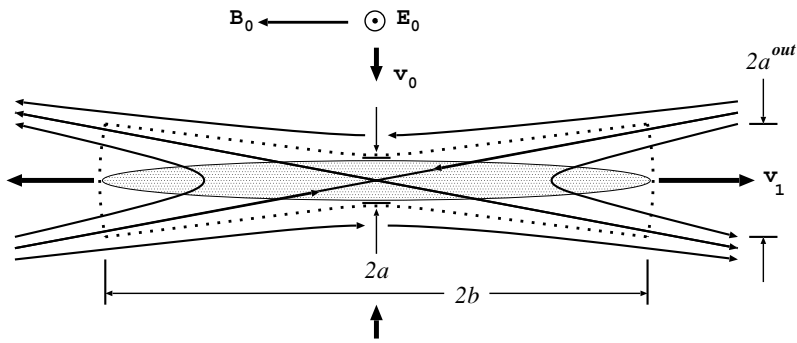
417

**Figure 1.** A super-hot turbulent-current layer (SHTCL) model: the electric current distribution is shown by the shadow, the dotted boundary indicates the field lines going through the current layer.

Because of the difference between the effective temperatures of electrons ($T_e = T$) and ions ($T_i = T/\theta$) in the outflowing plasma, the electron and ion thermal energy outflows also differ:

$$\mathcal{E}_{th,e}^{out} = \frac{5}{2}\, n_s k_\mathrm{B} T \cdot v_1 a^{out}\,, \qquad \mathcal{E}_{th,i}^{out} = \frac{5}{2}\, n_s k_\mathrm{B} \frac{T}{\theta} \cdot v_1 a^{out}\,. \tag{2.5}$$

The ion kinetic energy flux from the layer

$$\mathcal{K}_i^{out} = \frac{1}{2}\, M n_s v_1^2 \cdot v_1 a^{out} \tag{2.6}$$

is important in the energy balance (2.2). However, electrons play the dominant role in the anomalous heat-conductive cooling of the SHTCL, $\mathcal{C}_\parallel^{an}$.

In the typical conditions of solar flares, the effective temperature of electrons inside the SHTCL, $T_e \approx 100-200$ MK, and the power of energy release, $P \approx 10^{28} - 3 \times 10^{29}$ erg/s. For all particles with high enough velocities, the electric force exceeds the effective drag (due to wave-particle interactions) force, and they are able to run away from the quasi-thermal distribution (see Somov 2000). Thus, the SHTCL provides two components: the quasi-thermal super-hot plasma (Somov, Kosugi & Sakao 1998) and supra-thermal accelerated particles (Litvinenko & Somov 1991).

### 2.2. Particle acceleration in the SHTCL

Multi-wavelength observations of flares allows us to estimate the electric field related to reconnection: $E_0 \approx c^{-1} v_0 B_0 \gtrsim 10$ V/cm (e.g. Somov, Oreshina & Lubimov 2004). Litvinenko & Somov (1991) showed that acceleration by the electric field and scattering of electrons by turbulence in the SHTCL lead to appearance of about $10^{36}$ electrons with a power-law spectrum and with energies of the order of tens of keV. Therefore, the SHTCL model allows us to interpret the first step of electron acceleration in solar flares (Litvinenko & Somov 1993).

Acceleration of protons and heavier ions represents a more complicated problem because they are not so well magnetized by a magnetic field inside the SHTCL as electrons. In ordinary model of the SHTCL, the energy of ions does not exceed 10-20 MeV. A promising idea is that the charge-separation electric field detains protons in the vicinity of an electron current layer and increases the acceleration efficiency (Litvinenko & Somov 1995). Presumably this is a way to consider the SHTCL as a place of the proton pre-acceleration in flares.
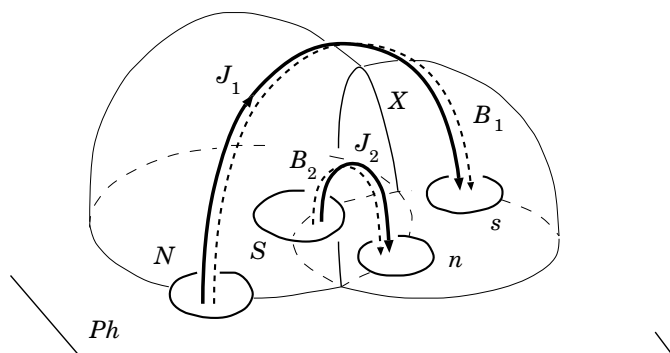
**Figure 2.** A 3D topological model of the coronal magnetic field in an active complex with four magnetic sources of interchanging polarities in the photosphere $Ph$ and with the two systems of currents in the corona.

### 2.3. *Magnetic reconnection of electric currents*

Reconnection reconnects field lines together with field-aligned currents. Hénoux & Somov (1987) considered reconnection between two currents $J_1$ and $J_2$ distributed inside two magnetic cells that interact along the separator $X$ in the corona as illustrated by figure 2. After reconnection, the currents will be connected in different electric circuits. Hence, reconnection changes the inductive energy of a global current system. In this way, a part of flare energy can be attributed to a change in the current pattern but not to a current dissipation.

Aschwanden et al. (1999) studied in detail the 3D quadrupolar reconnection in flares. One finding is that 6 out of 10 studied flares had the almost collinear reconnecting loops. A self-inductance of the largest loop involved in reconnection is relevant for the free magnetic energy in flares. The amount of the energy dependes on the length of this loop and the current ratio $J_1/J_2$.

### 2.4. *Rainbow reconnection model*

If a photospheric vortex flow with the velocity field **v** distorts the polarity inversion line (the neutral line $NL$) so that it takes the shape of the letter $S$, then a separator appears in the corona as shown in figure 3 (Somov 1985, 1986). The separator $X$ is located above the curve $NL$ like a rainbow above a river which makes a smooth bend. The vortex flow generates two components of the velocity: directed to the $NL$ and parallel to the $NL$. The first one tends to compress the photospheric plasma near the $NL$ and in such a way it can drive reconnection in the corona and photosphere. The second component provides a shear of magnetic field lines above the $NL$.

Before a large two-ribbon flare, like the Bastille-day flare on 2000 July 14, the magnetic separatrices are presumably involved in large-scale photospheric flows (which can be traced by proper motions of sunspots in an active region) of two types: (a) the converging flows induce the pre-flare current layers in the corona, (b) the shear flows make field lines longer, increasing the energy in the field.

During a flare, both excesses of magnetic energy are transformed in particle energy. Thus, the rainbow reconnection model predicts two kinds of apparent displacements of the footpoint (FP) bright HXR sources. First, an increase of a distance between the flare ribbons results from reconnection in a coronal RCL. The second effect is a decrease of the distance between the FP sources moving to each other as a result of shear relaxation (Somov et al. 2002). Both effects are well seen in figure 4.
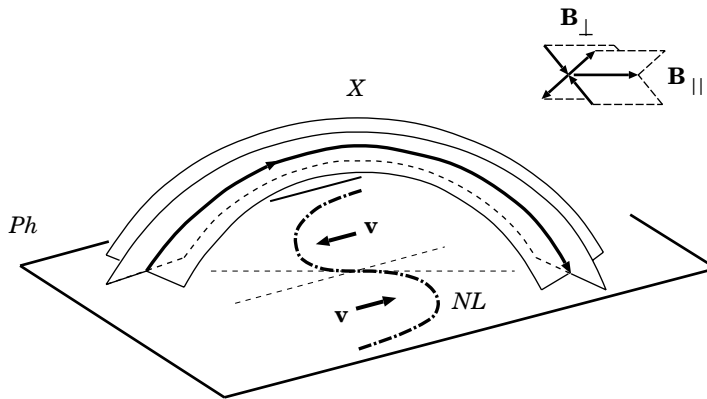
**Figure 3.** The separator $X$ above the $S$-shaped bend of the photospheric neutal line $NL$. The inset in the upper right-hand corner shows the structure of the magnetic field near the top of the separator.
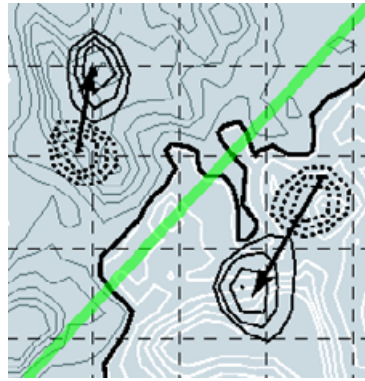


**Figure 4.** Position and motion of the footpoint HXR sources observed by the *Yohkoh* HXT (M2-band: 33-53 keV) in the M4.4 flare on 2000 October 29. The beginnings of arrows correspond to the time 01:46:49 UT, the ends are at 01:49:05 UT. The straight semi-transparent line represents the simplified netral line of the photospheric magnetic field observed by *SoHO* MDI.

## 3. The collapsing trap effects

Collapsing magnetic traps are formed by the process of collisionless reconnection in the solar atmosphere (Somov & Kosugi 1997). Figure 5 illustrates this possibility. Fast (figure 5$a$) and slow (figure 5$b$) modes of reconnection are shown. The electrons and ions preaccelerated in the SHTCL are captured in a trap whose length rapidly decreases.

The particle acceleration can be demonstrated in a simple model – a long trap with short mirrors (figure 6). The decreasing length $L(t)$ of the trap is much larger than the length $l_m$ of the mirrors; the magnetic field $\mathbf{B} = \mathbf{B}_1$ is uniform inside the trap but grows from $\mathbf{B}_1$ to $\mathbf{B}_2$ in the mirrors. The quantity $B_2/B_1$ is called the mirror ratio; the larger this ratio, the higher the particle confinement in the trap. The validity conditions for the model are discussed by Somov & Bogachev (2003).

### 3.1. *The first-order Fermi-type acceleration*

If the magnetic field inside the trap is assumed (for the sake of simplicity) to be uniform and constant, then the longitudinal momentum of a particle increases with a decreasing
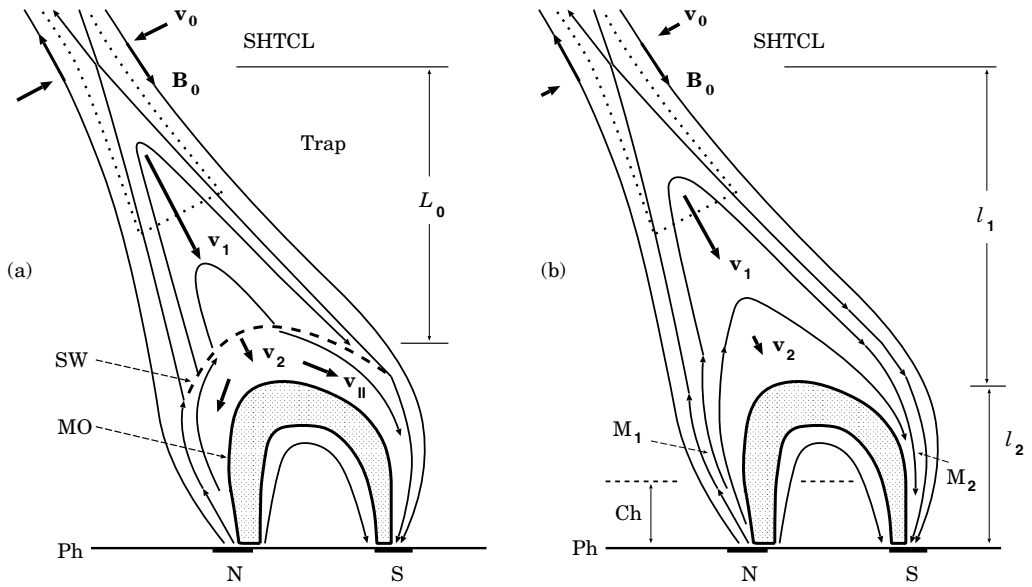
**Figure 5.** Flows of plasma related to the super-hot turbulent-current layer (SHTCL): the inflows with a relatively low velocity $\mathbf{v_0}$, the downward outflow with a super-Alfvén velocity $\mathbf{v_1}$. ($a$) SW is the shock wave above the magnetic obstacle (MO), the region of a strong magnetic field, which is observed in SXRs as a flare loop (shaded). $\mathbf{v_2}$ is the postshock velocity, $\mathbf{v_\parallel}$ is the velocity of spreading of the compressed plasma along the field lines toward the feet of the loop. ($b$) The supra-arcade downflow and collapsing trap without a shock. $M_1$ and $M_2$ are the mirroring points where the field becomes sufficiently strong to reflect fast particles above the chromosphere (Ch).

length $L(t)$, in the adiabatic approximation (Somov & Kosugi 1997), as

$$p_\parallel(l) = \frac{p_{0\parallel}}{l}, \tag{3.1}$$

where $l = L(t)/L_0$ is the dimensionless length of the trap. The transverse momentum is constant inside the trap,

$$p_\perp = p_{0\perp}, \tag{3.2}$$

because the first adiabatic invariant is conserved:

$$\frac{p_\perp^2}{B} = \text{const}. \tag{3.3}$$

Thus the kinetic energy of the particle increases as

$$\mathcal{K}(l) = \frac{p_\parallel^2 + p_\perp^2}{2\,m} = \frac{1}{2\,m}\left(\frac{p_{0\parallel}^2}{l^2} + p_{0\perp}^2\right). \tag{3.4}$$

The time of particle escape from the trap, $l = l_{es}$, dependes on the initial pitch-angle $\theta_0$ of the particle and is determined by the condition

$$\text{tg}\,\theta_0 = \frac{p_{0\perp}}{p_{0\parallel}} \leqslant \frac{1}{R\,l_{es}}, \tag{3.5}$$

where

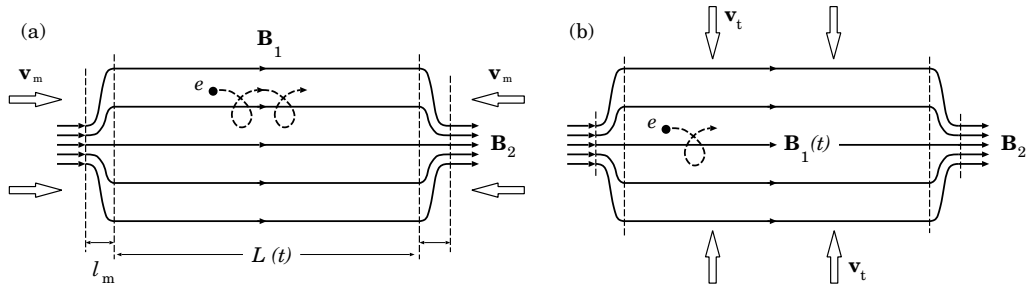$$R = \left(\frac{B_2}{B_1} - 1\right)^{1/2}. \tag{3.6}$$

**Figure 6.** Two effects in a collapsing trap. ($a$) Magnetic mirrors move toward each other with velocity $\mathbf{v}_m$. ($b$) Compression of the trap with velocity $\mathbf{v}_t$.

The kinetic energy of the particle at the time of its escape is

$$\mathcal{K}_{es} = \frac{p_{0\perp}^2}{2\,m}\left(R^2 + 1\right) = \frac{p_{0\perp}^2}{2\,m}\frac{B_2}{B_1}. \tag{3.7}$$

### 3.2. The betatron acceleration in a collapsing trap

If the thickness of the trap also decreases with its decreasing length, than the field $\mathbf{B}_1$ inside the trap increases as a function of $l$, say $B(l)$. In this case, according to (3.3), the transverse momentum increases simultaneously with the longitudinal momentum (3.1):

$$p_\perp(l) = p_{0\perp}\left(\frac{B(l)}{B_1}\right)^{1/2}. \tag{3.8}$$

Here $B_1$ is the initial (at $l = 1$) field inside the trap. The kinetic energy of a particle

$$\mathcal{K}(l) = \frac{1}{2\,m}\left(\frac{p_{0\parallel}^2}{l^2} + p_{0\perp}^2\,\frac{B(l)}{B_1}\right) \tag{3.9}$$

increases faster than that in the absence of trap contraction, see (3.4). Therefore, it is natural to assume that the acceleration efficiency in a collapsing trap also increases.

However, as the trap is compressed, the loss cone becomes larger (figure 7),

$$\theta_{es}(l) = \arcsin\left(\frac{B(l)}{B_2}\right)^{1/2}. \tag{3.10}$$

Consequently, the particle escapes from the trap earlier.

On the other hand, the momentum of the particle at the time of its escape satisfies the condition

$$p_\parallel(l) = R(l)\,p_\perp(l), \tag{3.11}$$

where

$$R(l) = \left(\frac{B_2}{B(l)} - 1\right)^{1/2}. \tag{3.12}$$

Hence, using (3.8), we determine the energy of the particle at the time of its escape from the trap

$$\mathcal{K}_{es} = \frac{p_\perp(l)^2}{2\,m}\left(R(l)^2 + 1\right) = \frac{p_{0\perp}^2}{2\,m}\frac{B(l)}{B_1}\frac{B_2}{B(l)} = \frac{p_{0\perp}^2}{2\,m}\frac{B_2}{B_1}. \tag{3.13}$$

The kinetic energy (3.13), that the particle gains in a collapsing trap with compression, is equal to the energy (3.7) in a collapsing trap without compression, i.e. without the betatron effect.
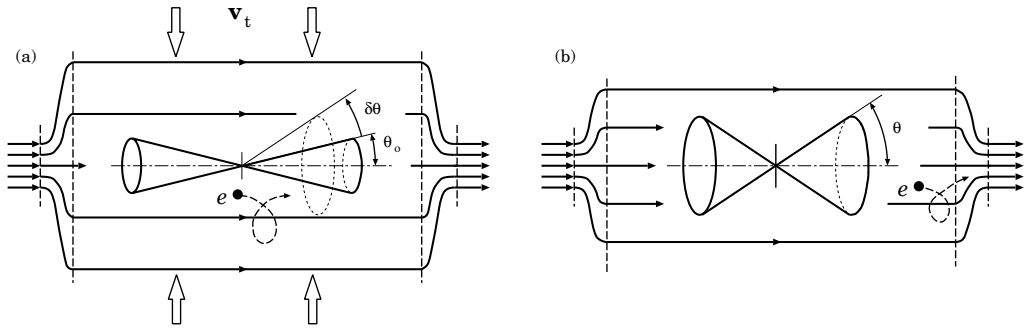
**Figure 7.** The betatron effect in a collapsing trap. ($a$) As the trap is conpressed with velocity $\mathbf{v}_t$, the loss cone becomes larger. ($b$) A particle escapes from the trap earlier with an additional energy due to betatron acceleration.

Thus, the compression of a collapsing trap (as well as its expansion or the transverse oscillations) does not affect the final energy that the particle acquires during its acceleration. The faster gain in energy is *exactly* offset by the earlier escape of the particle from the trap (Somov & Bogachev 2003). The acceleration efficiency, which is defined as the ratio of the final ($l = l_{ls}$) and initial ($l = 1$) energies, i.e.

$$\frac{\mathcal{K}_{es}}{\mathcal{K}(1)} = \frac{p_{0\perp}^2}{p_{0\perp}^2 + p_{0\parallel}^2} \frac{B_2}{B_1} = \left(\frac{p_{0\perp}}{p_0}\right)^2 \frac{B_2}{B_1}, \tag{3.14}$$

depends only on the ratio $B_2/B_1$ and the initial particle momentum or, to be more precise, on the ratio $p_{0\perp}/p_0$. The acceleration efficiency (3.14) does not depend on the compression of collapsing trap and the pattern of decrease in the trap length either.

It is of principal importance that the acceleration time in a collapsing trap with compression can be much shorter than that in a collapsing trap without compression. In this way, the betatron effect can significantly increase the actual efficiency of the main process – the particle acceleration on the converging magnetic mirrors.

### 3.3. *The betatron acceleration in a shockless trap*

If we ignore the betatron effect in a shockless collapsing trap, show in figure 5$b$, then the longitudinal momentum of a particle is defined by the formula (instead of (3.1))

$$p_\parallel(t) \approx p_\parallel(0) \frac{(l_1 + l_2)}{l_2 + (l_1 - v_1 t)} \Rightarrow p_\parallel(0) \frac{(l_1 + l_2)}{l_2}, \quad \text{when} \quad t \rightarrow t_1. \tag{3.15}$$

The particle acceleration on the magnetic mirrors stops at the time $t_1 = l_1/v_1$ at a finite longitudinal momentum that corresponds to a residual length ($l_2$ in figure 5$b$) of the trap.

Given the betatron acceleration due to compression of the trap, the particle acquires the same energy (3.7) by this time or earlier if the residual length of the trap is comparable to a critical length $l_{cr}$ determined by a compression law (see Somov & Bogachev 2003). Thus, the acceleration in shockless collapsing traps with a residual length becomes more plausible. The possible observational manifestations of such traps in solar flares are discussed by Somov & Bogachev (2003).

## 4. Conclusions

The observed motions of HXR emission at the FPs reflect the continuous reconnection, the most pronounced examples of which are the two-ribbon flares produced by reconnection at rising altitudes in corona according to the standard models (e.g. Sturrock 1966; Kopp & Pneuman 1976; Forbes & Acton 1996). However, the Yohkoh HXT observations show that actual solar flares are usually not so simple as the standard models predict.

Under actual conditions in the solar atmosphere, reconnection always occurs in a more complicated configuration of magnetic field: at least, in the presence of the field component which is parallel to the simplified neutral line in the photosphere. As a consequence, the other types of the footpoint HXR motions dominate in flares. They are better described by the rainbow reconnection model.

In order to interpret the temporal and spectral evolution and spatial distribution of HXRs in flares, a two-step acceleration was proposed by Somov & Kosugi (1997) with the second-step acceleration via the collapsing trap. Efficient trapping and continuous acceleration also produce the large flux and time lags of microwaves that are likely emitted by electrons with higher energies, several hundred keV (Nitta & Kosugi 1986; Kosugi, Dennis & Kai 1988).

Recently, Qiu, Lee & Gary (2004) presented a comprehensive study of the X5.6 flare on 2001 April 6. Evolution of HXRs and microwaves during the gradual phase in this flare exhibits a separation motion between two FPs, which reflects the progressive reconnection. The gradual HXRs have a harder and hardening spectrum compared with the impulsive component. The gradual component is also a microwave-rich event lagging the HXRs by tens of seconds. The authors propose that the collapsing-trap effect is a viable mechanism that continuously accelerates electrons in a low-density trap before they precipitate into the FPs.

### Acknowledgements

## References

Aschwanden, M. J., Kosugi, T., Hanaoka Y. et al. 1999 *Astrophys. J.* **526**, 1026–1045.
Forbes, T. G. & Acton, L. W. 1996 *Astrophys. J.* **459**, 330–340.
Hénoux, J.-C. & Somov, B. V. 1987 *Astron. Astrophys.* **185**, 306–314.
Kopp, R. A. & Pneuman, G. W. 1976 *Solar Phys.* **50**, 85–94.
Kosugi, T., Dennis, B. R. & Kai, K. 1988 *Astrophys. J.* **324**, 1118–1127.
Litvinenko, Y. E. & Somov, B. V. 1991 *Soviet Astronomy Lett.* **17**, 353–356.
Litvinenko, Y. E. & Somov, B. V. 1993 *Solar Phys.* **146**, 127–133.
Litvinenko, Y. E. & Somov, B. V. 1995 *Solar Phys.* **158**, 317–330.
Nitta, N. & Kosugi, T. 1986 *Solar Phys.* **105**, 73–82.
Qiu, J., Lee, J. & Gary, D. E. 2004 *Astrophys. J.* **603**, 335–347.
Somov, B. V. 1985 *Soviet Physics - Usp.* **28**, 271–272.
Somov, B. V. 1986 *Astron. Astrophys.* **163**, 210–218.
Somov, B. V. 2000 *Cosmic Plasma Physics*, Kluwer Academic Publ., Dordrecht.
Somov, B. V. & Bogachev, S. A. 2003 *Astronomy Lett.* **29**, 621–628.
Somov, B. V. & Kosugi, T. 1997 *Astrophys. J.* **485**, 859–868.
Somov, B. V., Kosugi, T. & Sakao, T. 1998 *Astrophys. J.* **497**, 943–956.
Somov, B. V., Kosugi, T., Hudson H. S. et al. 2002 *Astrophys. J.* **579**, 863–873.
Somov, B. V., Kosugi, T., Hudson H. S. et al. 2003 *Adv. Space Res.* **32**, No. 12, 2439–2450.
Somov, B. V., Oreshina, I. V. & Lubimov, G. P. 2004 *Astronomy Rep.* **48**, 246–253.
Sturrock, P. A. 1966 *Nature* **211**, No. 5050, 695–697.